Electrically Controlled Phased Array OAM Radar

Daniel J. Orfeo^a, Dylan Burns^a, Dryver R. Huston^a, Tian Xia*^b
^aUniversity of Vermont Dept. of Mechanical Engineering, Burlington VT 05405; ^bUniversity of Vermont Dept. of Electrical and Biomedical Engineering, Burlington VT 05405

ABSTRACT

Control of orbital angular momentum (OAM) offers the potential for increases in control, sensitivity, and security for high-performance microwave systems. OAM is characterized by an integer OAM mode where zero represents the case of a plane wave. Microwaves with a nonzero OAM mode propagate with a helical wavefront. Orthogonal OAM modes can be used to carry distinct information at the same frequency and polarization, increasing the data rate. The OAM waveform may also increase radar detection capability for certain shaped objects. OAM can be induced by broadcasting a plane wave through a spatial phase plate (SPP) dielectric which introduces an azimuthally dependent phase delay. However, SPPs are frequency-specific, which presents an obstacle for harnessing OAM in frequency-modulated communication systems and wide-bandwidth radar. In this study, we develop a circular phased array to synthesize the desired vortex-shaped wavefront. This approach offers a critical advantage: the phases of all antenna elements are easily programmable under different frequencies. As a result, transmission and reception of the OAM beam can be controlled with great flexibility, making it operable over a wide frequency spectrum, which leverages OAM radar functionality and performance. In this paper, we will investigate a wide-bandwidth radar with OAM mode-control and signal processing.

Keywords: phased array, orbital angular momentum, OAM, radar, gprMax, finite-difference time-domain

1. INTRODUCTION

1.1 Orbital Angular Momentum for Microwave Sensing

Antenna orientation has a significant effect on signal returns for conventional penetrating microwave radars [1]. Light can be twisted into a helical structure, providing additional degrees of freedom that conventional microwave systems do not use. Light with this helical structure has nonzero orbital angular momentum (OAM). Electronic control of OAM offers the potential for increases in sensitivity, spectral efficiency, and security for high-performance microwave systems. EM beams, including beams with OAM, can be interpreted at the quantum level as photons, or at the macroscopic level with Maxwell's equations [2]. This investigation considers the macroscopic interpretation. Each OAM mode has a helical geometry, with the integer mode number corresponding to the number of intertwined helices [3]. A plane wave represents OAM mode 0. OAM modes are mutually orthogonal and can be used to carry distinct information at the same frequency and polarization [4], increasing the data rate [5]. Certain object shapes or arrangements may be easier to detect using a radar operating with a specific OAM mode, due to unique scattering properties of waveforms with OAM [6]. Some Bessel beams can overcome partial obstruction due to a self-compensating diffraction [7]. There is evidence to suggest OAM waveforms may have a similar self-healing property [8]. OAM can be induced in microwaves by broadcasting a plane wave through a spatial phase plate (SPP) dielectric which introduces an azimuthally dependent phase delay [9, 10], as shown in Figure 1(a). However, SPPs are frequency-specific, which presents an obstacle for harnessing OAM in frequency-modulated communication systems and wide-bandwidth radar. Figure 1(b) shows a circular phased array which synthesizes the desired vortex-shaped wavefront [11, 12]. This approach offers a critical advantage: the phases of all antenna elements are programmable under different frequencies. As a result, transmission and reception of an OAM beam can be controlled across a wide frequency bandwidth.

1.2 Laguerre-Gaussian modes for OAM

OAM modes can be described by an orthogonal decomposition of Laguerre-Gaussian modes. The generalized Laguerre polynomials for an arbitrary and real α are the polynomial solutions of the following [13] differential equation:

$$xy'' + (\alpha + 1 - x)y' + ny = 0 (1)$$

^{*}txia@uvm.edu; 1-802-656-8996

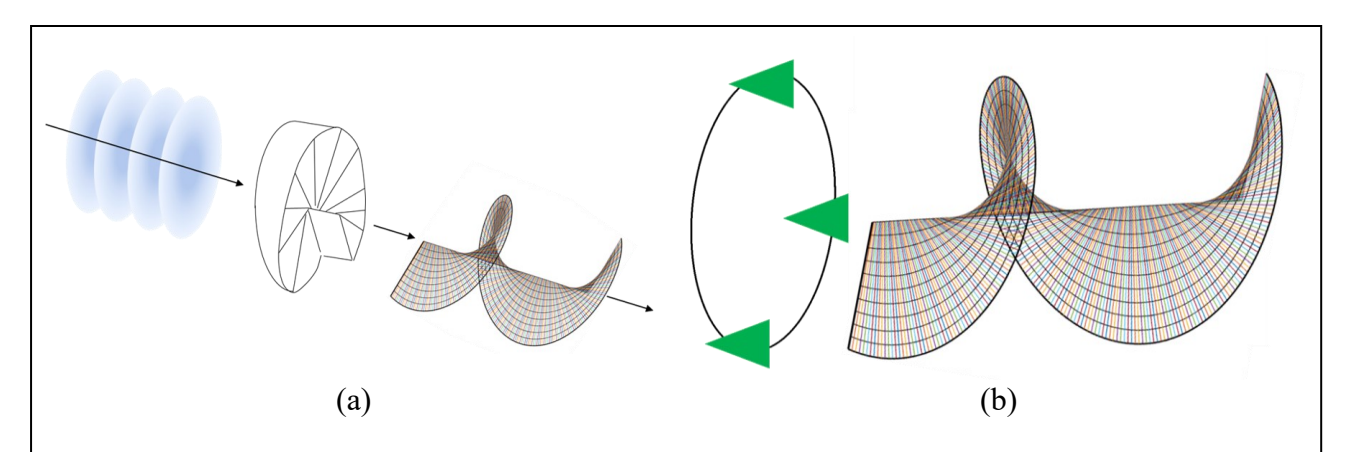


Figure 1 (a) OAM is induced by broadcasting a plane wave through a spatial phase plate (SPP) dielectric which introduces an azimuthally dependent phase delay. (b) An OAM (l=-1) electromagnetic wave propagating from a three-antenna circular phased array of microwave antennas.

The beam profiles are solved using the Laguerre-Gaussian modal decomposition. These functions are written in cylindrical coordinates [14] using generalized Laguerre polynomials:

$$u(r,\phi,z) = C_{lp}^{LG} \frac{w_0}{w(z)} \left(\frac{r\sqrt{2}}{w(z)}\right)^{|l|} \exp\left(-\frac{r^2}{w^2(z)}\right) L_p^{|l|} \left(\frac{2r^2}{w^2(z)}\right) \times \exp\left(-ik\frac{r^2}{2R(z)}\right) \exp(-il\phi) \exp(i\psi(z))$$
 (2)

where C_{lp}^{LG} is a required normalization constant [15]:

$$C_{lp}^{LG} = \sqrt{\frac{2p!}{\pi(p+|l|)!}} \Rightarrow \int_0^{2\pi} d\phi \int_0^\infty r dr |u(r,\phi,z)|^2 = 1$$
 (3)

2. PHASED ARRAYS FOR ORBITAL ANGULAR MOMENTUM

2.1 Vector Potential for a Continuous Emitter

Consider a potential formulation of Maxwell's equations where **A** is the vector potential and thereby the curl of **A** is the magnetic field **B**: $\nabla \times \mathbf{A} = \mathbf{B}$. This gives Maxwell's equations in terms of the magnetic vector potential **A** and the electric scalar potential ϕ . For sufficiently large N, the circular array can be idealized as a continuous circular emitter [16]:

$$\mathbf{A}(\mathbf{r}) \approx \frac{-\mu_0 \omega \mathbf{j} d}{4\pi} \frac{e^{ikr}}{r} N \mathbf{i}^{-l} e^{il\varphi} J_l(ka \sin \theta)$$
 (4)

where a is the radius of the circular phased array, d is electric dipole length, \mathbf{j} is the constant current density vector, J_l is a Bessel function of the first kind, \mathbf{k} is the wave vector magnitude λ^{-1} , l is OAM mode number, μ_0 is vacuum permeability, and ω is circular frequency. MATLAB was used to numerically model the phase front for the continuous circular emitter is shown in Figure 2(a). In this calculation radius $a=\lambda$, frequency f=3 GHz, and OAM mode l=1. These values were chosen to be realistic for a ground penetrating radar application, and for comparison with work published by Mohammadi et al. [17, 18] and Liu et al. [16]. Figure 2(b) shows the spiral-shaped phase front of (A) for the continuous circular emitter. The view is shown at 25λ in front of the array, and the visible window has dimensions 40λ by 40λ . The phase is shown from $-\pi$ (blue) to π (red).

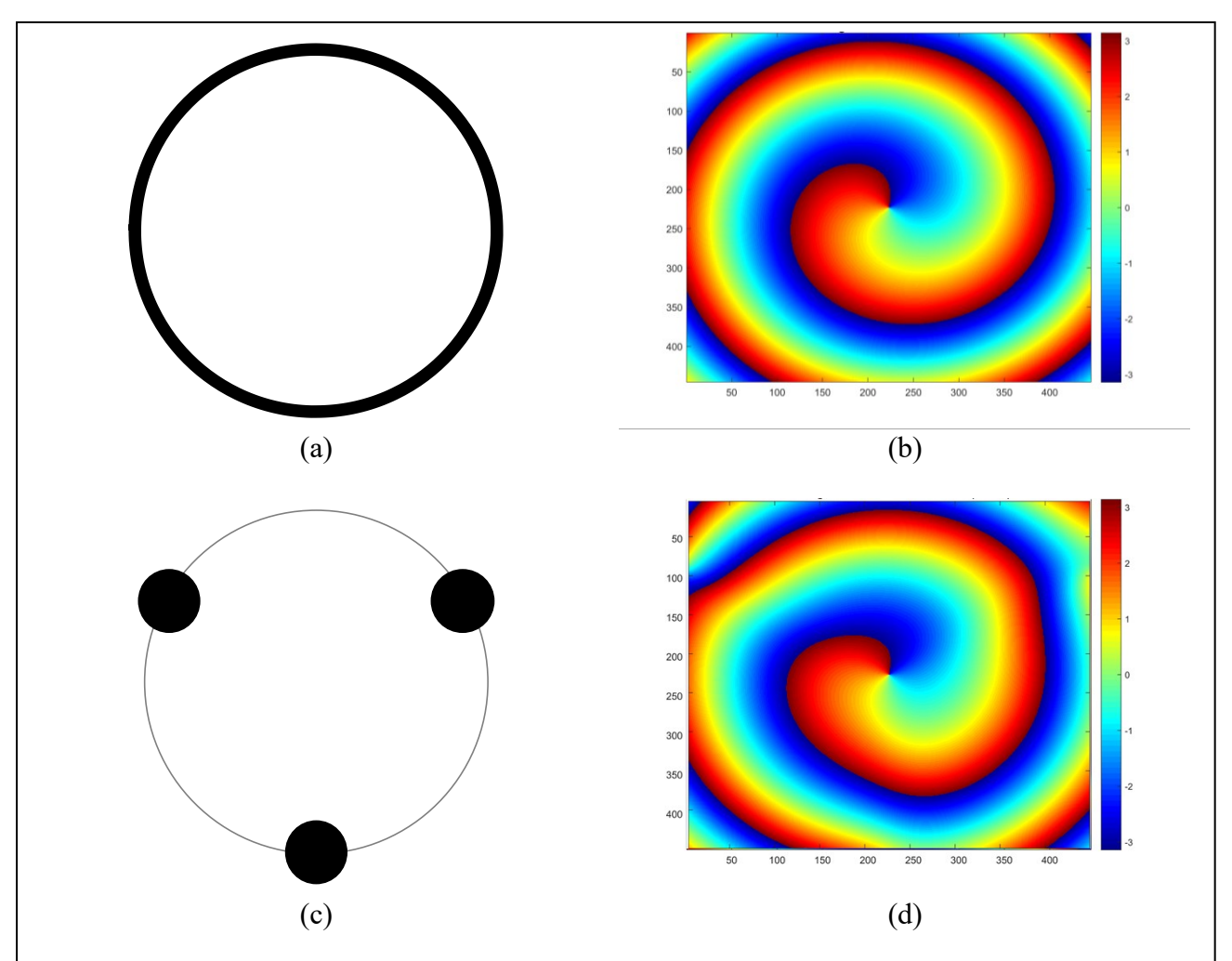


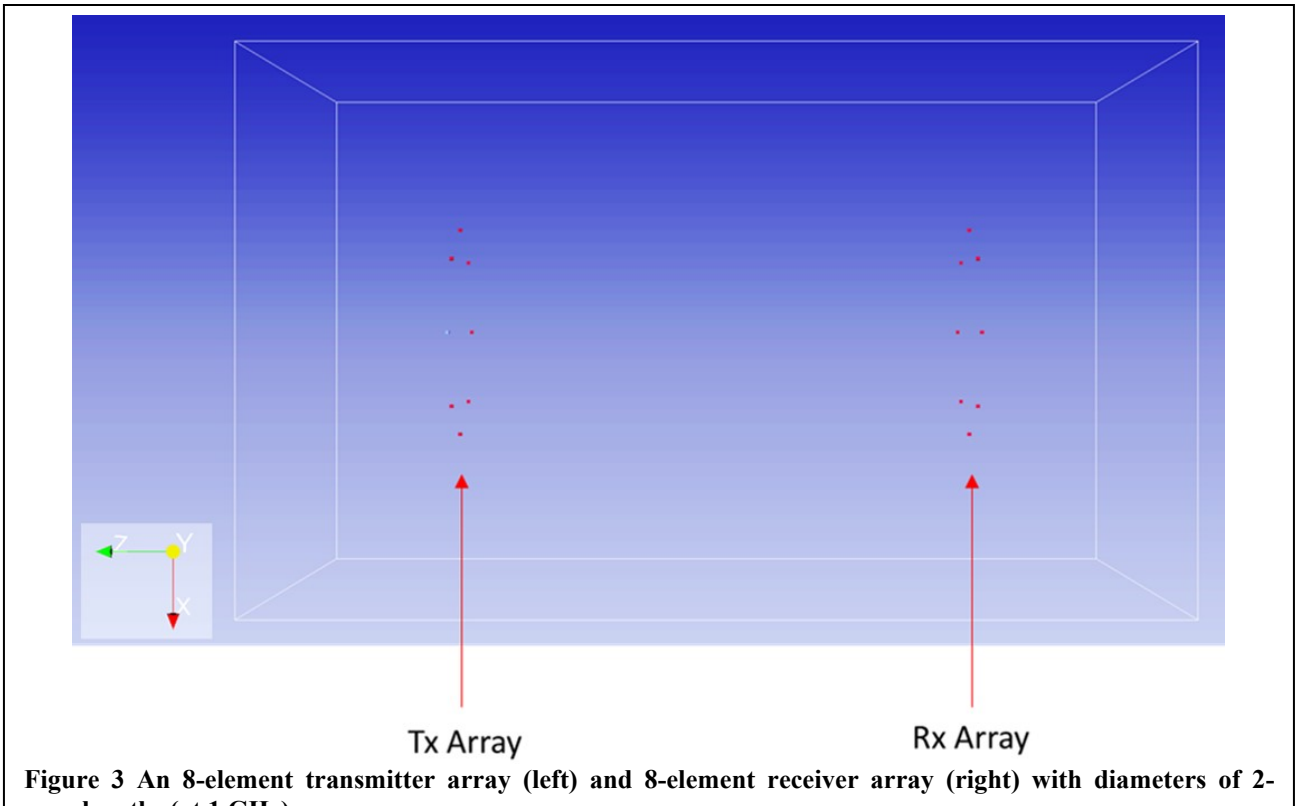
Figure 2 (a) A circular phased array approximated as continuous circular emitter. (b) The phase front of A for this continuous emitter. (c) A circular phased array with N=3 antennas. (d) The phase front of A for this array with N=3 antennas.

2.2 Vector Potential for a Circular Phased Array

The continuous emitter assumption may not always be applicable, however. Gigahertz-frequency microwave antennas have non-trivial physical dimensions which limits the number of antenna elements which can be placed in a circular phased array. Furthermore, high-quality multichannel microwave equipment is often expensive, which places practical limits on the number of antennas used in many research applications. Because of this, a discrete model is considered which can model the vector potential created by a relatively small number of phased array antenna elements. The vector potential (A) for an circular array of N antennas [16] can be expressed:

$$\mathbf{A}(\mathbf{r}) \approx \frac{-\mu_0 \omega \mathbf{j} d}{4\pi} \frac{e^{\mathrm{i}kr}}{r} \sum_{n=1}^{N} e^{-\mathrm{i}(k\mathbf{r}_n - l\varphi_n)}$$
 (5)

A phased array with many individual antenna elements should closely approximate the continuum case and produce a high-quality waveform. But what about an array with few antennas? The antenna arrangement for the *N*=3 case is shown in Figure 2(c), and the phase front of the vector potential generated by this array is shown in Figure 2(d). The same modeling parameters are used as for the continuous emitter model in Figure 3(b). Despite some triangularization, the vector potential shown in Figure 3(d) exhibits the same overall phase front structure as the continuous emitter result. While this



wavelengths (at 1 GHz)

does not prove that it is possible to generate an OAM l=1 mode with only three antennas, it does provide evidence that sparse arrays may be a viable path forward for transmitting microwaves with OAM characteristics.

3. FINITE-DIFFERENCE TIME-DOMAIN SIMULATION

3.1 gprMax Model Specifications

Finite-Difference Time-Domain (FDTD) simulations were performed using the program gprMax [19] to model OAM waveform characteristics. An 8-element transmitter array and 8-element receiver array with diameters of 2-wavelengths (at 1 GHz) were modeled, as shown in Figure 3. Each antenna in the transmitting array broadcasts a phase-adjustable 1 GHz sine wave. The simulation domain is 1.5 x 1.5 x 2.5 meters, including a 0.25-meter thick Perfectly Matched Layer (PML) absorbing boundary condition on each face. The time step is 6.16 picoseconds, with a 9.9 nanosecond simulation duration. Spatial resolution in the X, Y, and Z directions is 3.2 millimeters. To verify model function, a single sine wave is simulated. This sine wave is transmitted from one Y-direction polarized antenna in the transmitter array and X, Y, and Z components of this waveform are received at each of the eight receiver antennas. The Y-direction components are selected, and a moving-mean filter is applied to each of the received signals to remove high-frequency noise. These data are plotted in Figure 4(a). Due to geometric path-lengths between antenna elements, three pairs of signals overlap exactly. Because of this, five sine waves are visible in the plot.

3.2 OAM Modes

To simulation waveforms with different OAM modes, sine waves are transmitted from all 8 antennas in the transmitter array and received by all 8 antennas in the receiver array. In Figure 4(b), all eight sine waves are transmitted with the same phase, to produce an OAM 0 (plane wave) waveform. The received Y-component signals are smoothed by a moving-mean filter and plotted. Due to geometric path-lengths, all eight signals overlap almost exactly. In Figure 4(c), sine waves are transmitted with phase delays to produce an OAM +1 (left-handed single helix) waveform. The received Y-component signals are smoothed by a moving-mean filter. Left-handedness is shown by the signal order, from left to right in the plot:

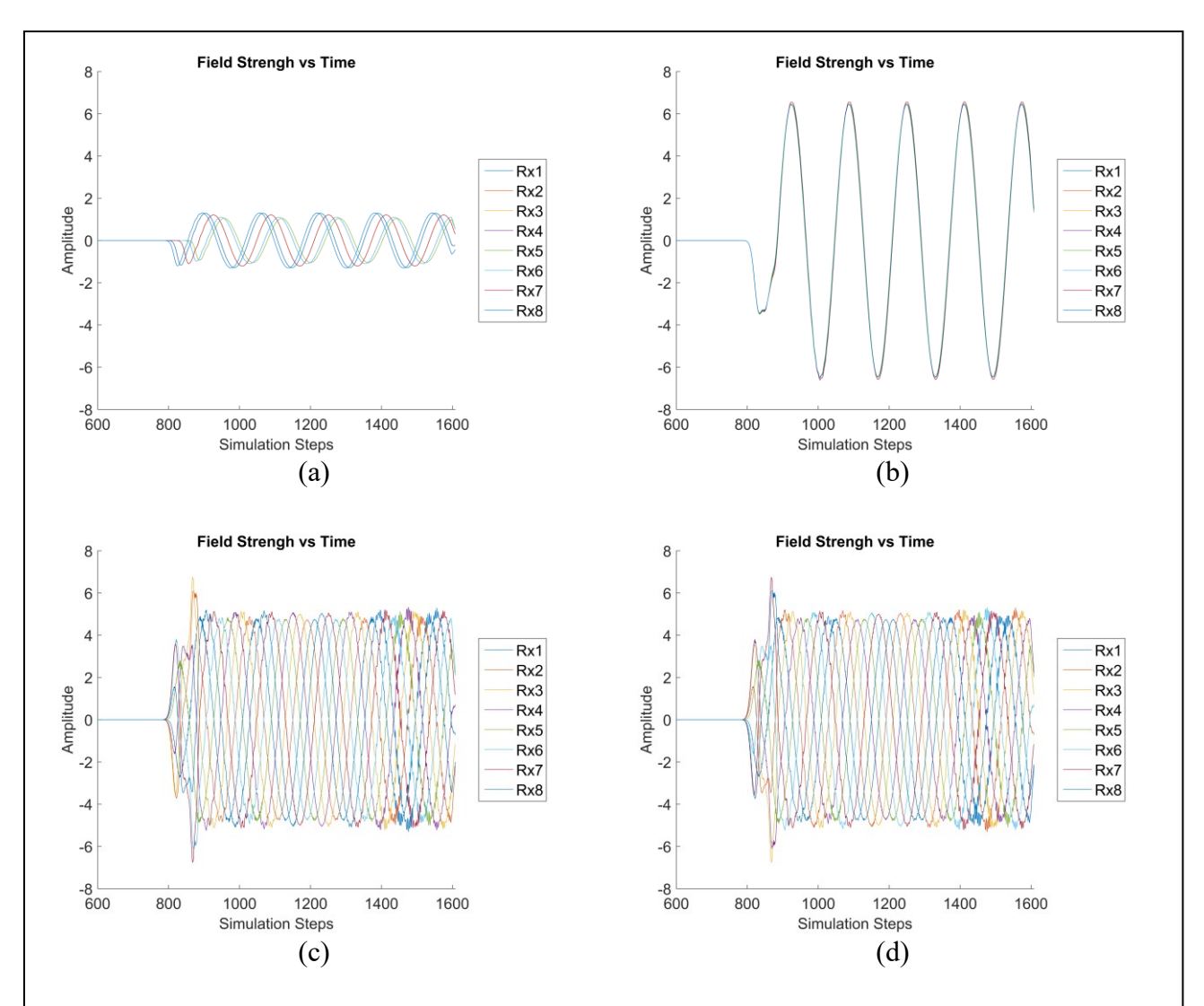


Figure 4 (a) A single sine wave is transmitted from one antenna in the transmitter array and received by all 8 antennas in the receiver array. (b) In-phase sine waves are transmitted from all 8 antennas in the transmitter array and received by all 8 antennas in the receiver array (OAM 0). (c) Eight sine waves are transmitted with phase delays to produce an OAM +1 (left-handed single helix) waveform. (d) Eight sine waves are transmitted with phase delays to produce an OAM -1 (right-handed single helix) waveform.

Rx8, Rx7, Rx6, Rx5, Rx4, Rx3, Rx2, Rx1. Figure 4(d) shows sine waves transmitted with phase delays to produce an OAM -1 (right-handed single helix) waveform. The received Y-component signals are once again smoothed by a moving-mean filter. Right-handedness is shown by signal order, from left to right: Rx1, Rx2, Rx3, Rx4, Rx5, Rx6, Rx7, Rx8. Therefore, the left-to-right order of the received signals allows discrimination of OAM mode 0, OAM mode +1, and OAM mode -1. The ability to receive and distinguish OAM modes demonstrates the concept of Gigahertz-frequency OAM-mode modulated information transmission.

3.3 OAM Waveform Scattering

The FDTD method in gprMax was also used to simulate OAM waveform scattering. Figure 5(a) shows the 8-element transmitter array and 8-element receiver array with diameters of 4-wavelengths (at 1 GHz) that were modeled. Antennas are polarized in the Z-direction. The receiver array is oriented perpendicularly compared to the transmitter array to measure signal scattering. As before, each antenna in the transmitting array broadcasts a phase-adjustable 1 GHz sine wave. The simulation domain is 4.5 x 2 x 4.5 meters, including a 0.25-meter thick Perfectly Matched Layer (PML) absorbing

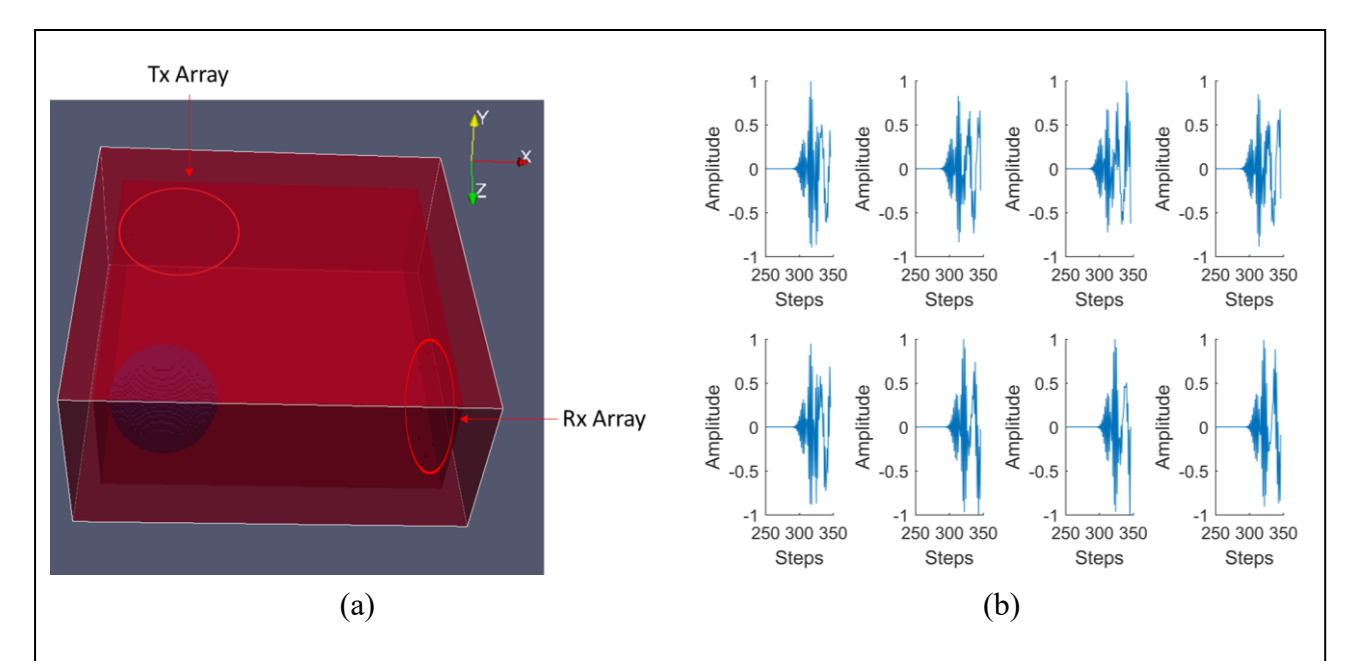


Figure 5 (a) An 8-element Z-polarized transmitter array and 8-element receiver array. Circles indicate the locations of transmitter and receiver arrays. Simulations were performed with and without a spherical Perfect Electric Conductor target, shown in blue. (b) The Z-components of the signal difference between a simulation with the spherical PEC target, and a simulation without the target.

boundary condition on each face. Here, the time step is approximately 56.9 picoseconds, and spatial resolution in the X, Y, and Z directions is 30 millimeters. The simulation duration is 19.9 nanoseconds. Two simulations were performed: one with a spherical Perfect Electric Conductor (PEC) target (shown in blue in Figure 5(a)), and one without the spherical PEC target. The spherical PEC target diameter is 120 cm (4-wavelengths at 1 GHz). In both simulations, sine waves were transmitted with phase delays to implement an OAM mode +1 waveform. Figure 5(b) shows the difference in received signals (Z-polarized component), when comparing the two simulations. This shows the portion of the OAM mode +1 waveform which is scattered due to the presence of the spherical PEC target. Note that the beginning of the simulation duration shows zero signal amplitude—this is because of the time it takes for the scattered waveform to reach the receiver array. Future work will attempt to characterize the unique scattering properties of waveforms, like this one, with nonzero OAM mode.

4. SYNTHETIC OAM

4.1 Wideband OAM with Network Analyzer

The ability to operate over a wide frequency bandwidth is necessary for high-resolution radar imaging. A method is proposed to provide wide bandwidth capability for an OAM radar. A 4-channel Keysight PNA-X N5241A network analyzer is used with wide bandwidth frequency-domain operation from 10 MHz to 13.5 GHz. This test setup is shown in Figure 6. For each pair-combination of the four antennas in the circular transceiver array, magnitude and phase data are recorded for frequencies from 10 MHz to 13.5 GHz. This gives sixteen antenna-pair measurement combinations of magnitude and phase at each sampled frequency: S₁₁, S₁₂... S₄₃, S₄₄. In particular, S₁₁, S₂₂, S₃₃, S₄₄ represent perpendicular reflections in which a signal is transmitted, reflects from a target, and is then received by the same antenna. This gives interpretable information about the phase distribution of the spatially structured OAM waveform. However, due to hardware limitations of the network analyzer, simultaneous transmission and reception of multiple channel combinations is not possible, and phase delays cannot be set on the transmission-side. This means that a true OAM waveform cannot be created. Instead, individual measurements are taken one-at-a-time, and helical OAM phasing is introduced automatically in post processing. If superposition is valid [20, 21] in time and free space, it may still be possible to extract useful information from such a test, provided complete (i.e., complex) magnitude and phase information is present. Leveraging superposition in this manner via post-processing gives synthetic OAM capabilities.

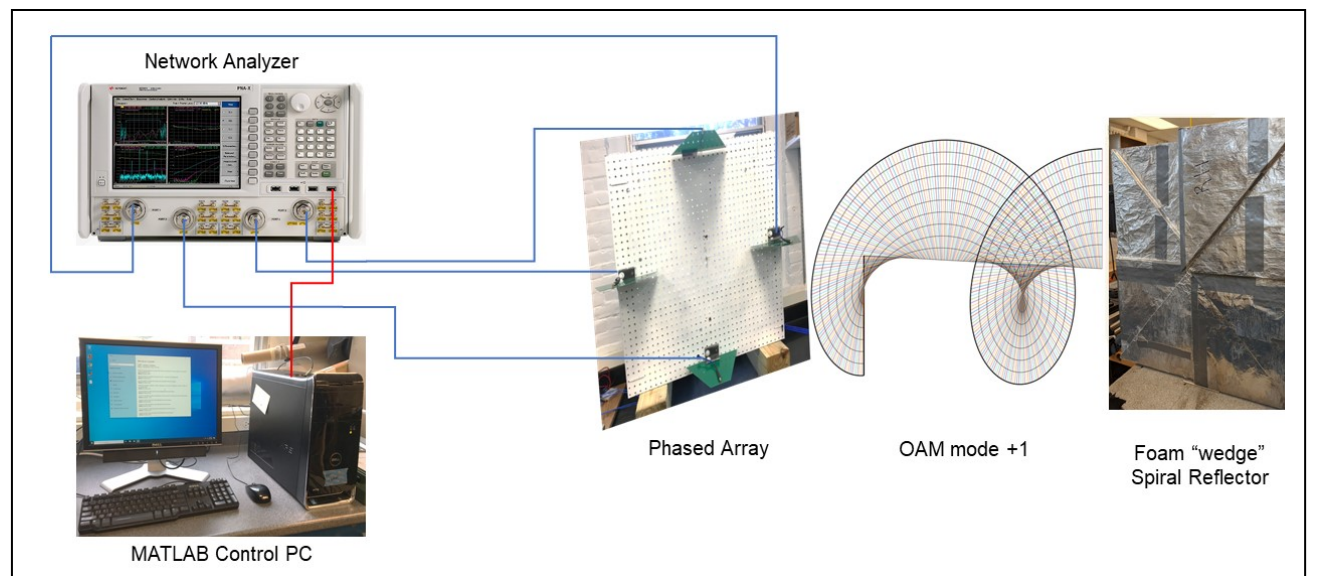


Figure 6 Synthetic wideband OAM with network analyzer and four-antenna circular transceiver array. A spiral reflector made of aluminum-covered wedges allows for detection of OAM.

4.2 Detecting OAM with a Spiral-Shaped Reflector

A test was devised to determine if the synthetic OAM waveforms exhibit the same scattering characteristics as OAM waveforms produced by a simultaneously transmitting phased array. The idea is to detect nonzero OAM modes with a spiral reflector. If the synthesized OAM waveform behaves like a true simultaneous OAM waveform, a spiral reflector will alter the phases of the reflected signals in a specific way. Then, if phase delays for the correct OAM mode are implemented in post processing, the received signal will be demodulated into a plane wave (OAM mode 0). This spiral reflector is chosen with pitch half that of the incident OAM helix, to account for the round-trip path of a reflected signal. For example, a right-handed (OAM -1) reflector demodulates a left-handed (OAM +1) waveform [12], as shown in Figure 6. Demodulation is advantageous because S₁₁, S₂₂, S₃₃, and S₄₄ measurements of plane wave signals can be summed to enhance signal-to-noise of the target. An increase in combined signal strength therefore provides confirmation of a particular OAM mode present in the incident (transmitted) signal. It is important to note that like a spiral phase plate, a spiral target must be tuned to a specific frequency. Because of this, $S_{11} + S_{22} + S_{33} + S_{44}$ signal strength will only increase at the frequency for which the spiral reflector is tuned, even when a wide bandwidth OAM frequency sweep is performed. However, there is no reason for OAM to occur only at an arbitrarily chosen frequency, and so detecting OAM characteristics at one frequency provides evidence that these characteristics will persist at the other frequencies within the frequency sweep. In this way, this test is used to determine whether or not the synthetic OAM waveform exhibits true OAM behavior. A successful test would indicate that the properties of an OAM signal can be reproduced by synthetically combining individual magnitude and phase measurements. If true, a network analyzer could be used as a wide bandwidth OAM radar.

4.3 Synthetic OAM Test

In a laboratory test, left and right-handed spiral reflector targets are tuned for an incident waveform frequency of approximately 1.2 GHz. Each target is designed to demodulate a specific OAM mode (+1 or -1) at 1.2 GHz. Adding the phase delays for the corresponding OAM mode will lead to OAM demodulation and increase the signal magnitude around 1.2 GHz when measuring the sum of the $S_{11} + S_{22} + S_{33} + S_{44}$ signals. Adding improper phase delays (or no phase delays) will fail to demodulate the OAM waveform, and lead to a degradation of the $S_{11} + S_{22} + S_{33} + S_{44}$ signal magnitude. We therefore expect a higher signal magnitude around 1.2 GHz: for the left-handed (OAM +1) target when the incident signal is post-processed with OAM -1 phasing, and for the right-handed (OAM -1) target when the incident signal is post-processed with OAM +1 phasing. Figure 7 shows the results for this test: X-axes indicate frequency, and Y-axes indicate signal magnitude. Vertical black lines indicate the region of interest around 1.2 GHz. Figure 7(a) and Figure 7(b) show the left-handed spiral target at distances of one and two meters, respectively. Signal magnitude near 1.2 GHz increases when the incident signal is post-processed with OAM -1 phasing. Figure 7(c) and Figure 7(d) show the right-handed spiral

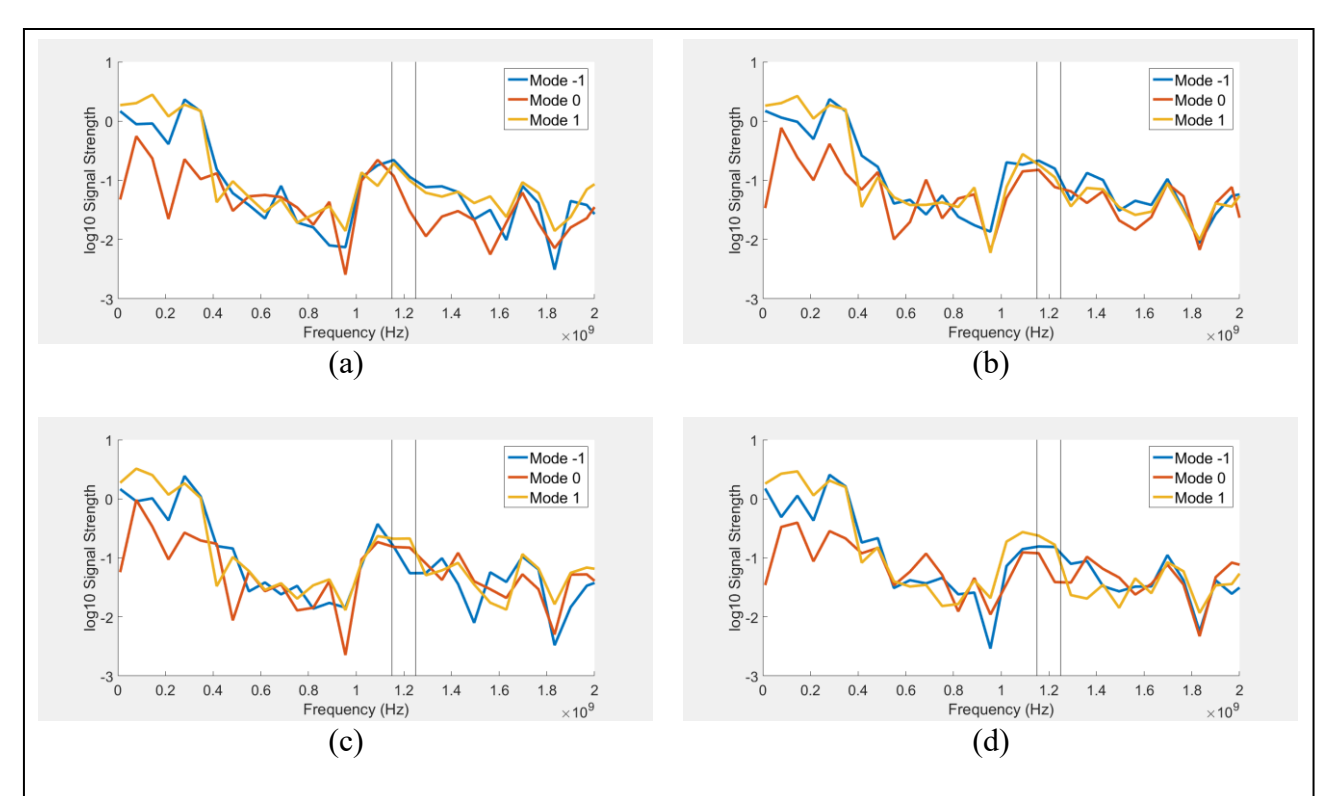


Figure 7 $S_{11} + S_{22} + S_{33} + S_{44}$ signal magnitudes. (a) The left-handed spiral target at a 1-meter distance. Signal magnitude near 1.2 GHz is greatest when the incident signal is post-processed with OAM -1 phasing. (b) The left-handed spiral target at a 2-meter distance. Signal magnitude near 1.2 GHz is greatest when the incident signal is post-processed with OAM -1 phasing. (c) The right-handed spiral target at a 1-meter distance. Signal magnitude near 1.2 GHz is greatest when the incident signal is post-processed with OAM +1 phasing. (d) The right-handed spiral target at a 2-meter distance. Signal magnitude near 1.2 GHz is greatest when the incident signal is post-processed with OAM +1 phasing.

target at distances of one and two meters. As expected, signal magnitude near 1.2 GHz increases when the incident signal is post-processed with OAM +1 phasing. This indicates successful functioning of the synthetic OAM system.

5. SUMMARY OF RESULTS

The results of this inquiry are summarized as follows. The continuous phase front of the vector potential (A) of an OAM waveform can be approximated using a circular phased array of as few as three discrete antenna elements. This provides motivation for performing microwave simulations and laboratory tests using circular phased arrays with four to eight elements. A circular phased array is then used in a simulation model of a gigahertz-frequency waveform with nonzero orbital angular momentum. In this simulation, gigahertz-frequency OAM modes (-1,0,+1) can be received and distinguished, demonstrating the concept of OAM-mode modulated information transmission. In addition, simple OAM waveform scattering is simulated for the case of a spherical target. Finally, a laboratory experiment is presented in which signal post processing is used to demonstrate the function of a synthetic wideband OAM radar using a network analyzer. It is found that combining individual magnitude and phase measurements can reproduce the behavior of OAM waveforms generated by a simultaneously transmitting phased array. This indicates that a system based on a network analyzer may be a viable path forward for the development of a wideband OAM radar.

6. CONCLUSIONS

The overarching goal of this research is to harness OAM in frequency-modulated communication systems and wide-bandwidth radar. In the synthetic OAM tests, the concept of a spiral phase plate dielectric lens has been adapted to a spiral reflector used to detect a specific OAM mode at a specific frequency. In this post-processing approach, the phases of all

antenna elements in a circular array are easily programmable under different frequencies. This flexibility is intended to advance the creation of an OAM radar with functionality and high performance over a wide frequency spectrum. Future work will focus on wideband and dual-function sensing and communication systems [22] which leverage the unique modulation and scattering potential of OAM waveforms.

ACKNOWLEDGEMENTS

This work has been supported by Defense University Research Instrumentation Program (DURIP) U.S. Army contract no. W911NF1810193, U.S. Army contract W909MY-17-C-0020 with White River Technologies, Inc., U.S. National Science Foundation grants 1647095 and 1640687, University of Vermont SPARK Fund, UVM Office for the Vice President for Research, and the Vermont Space Grant Consortium under NASA Cooperative Agreement NNX15AP86H.

REFERENCES

- [1] D. Orfeo, Y. Zhang, D. Burns, J. S. Miller, D. R. Huston, and T. Xia, "Bistatic antenna configurations for airlaunched ground penetrating radar," *Journal of Applied Remote Sensing*, vol. 13, no. 2, pp. 1-9, 9, 2019.
- [2] R. K. Wangsness, *Electromagnetic Fields*. New York: John Wiley & Sons, 1986.
- [3] T. Yuan, H. Wang, Y. Cheng, and Y. Qin, "Electromagnetic Vortex-Based Radar Imaging Using a Single Receiving Antenna: Theory and Experimental Results," (in eng), *Sensors (Basel)*, vol. 17, no. 3, Mar 19 2017.
- [4] L. Cheng, W. Hong, and Z.-C. Hao, "Generation of electromagnetic waves with arbitrary orbital angular momentum modes," *Scientific reports*, vol. 4, p. 4814Accessed on: 2014. doi: 10.1038/srep04814 Available: https://www.ncbi.nlm.nih.gov/pmc/articles/pmid/24770669/pdf/?tool=EBI
- [5] NASA, "2019 NASA Space Technology Research Fellowship (NSTRF19)," in NASA Technology Area 5.2.1: "Spectrum-Efficient Technologies", ed: NASA, 2019.
- [6] T. Omatsu, K. Masuda, K. Miyamoto, K. Toyoda, N. Litchinitser, Y. Arita, and K. Dholakia, "Twisted mass transport enabled by the angular momentum of light," *Journal of Nanophotonics*, vol. 14, p. 1, 03/18 2020.
- [7] J. Du and J. Wang, "High-dimensional structured light coding/decoding for free-space optical communications free of obstructions," *Optics Letters*, vol. 40, no. 21, pp. 4827-4830, 2015/11/01 2015.
- [8] D. Orfeo, D. Burns, T. Xia, and D. Huston, "Phased Array for Control of Orbital Angular Momentum in Microwave Systems," in *2019 IEEE International Symposium on Phased Array Systems and Technology*, Waltham, Massachusetts, 2019: IEEE Conference Proceedings.
- [9] M. Pu, X. Li, X. Ma, Y. Wang, Z. Zhao, C. Wang, C. Hu, P. Gao, C. Huang, H. Ren, X. Li, F. Qin, J. Yang, M. Gu, M. Hong, and X. Luo, "Catenary optics for achromatic generation of perfect optical angular momentum," *Science Advances*, vol. 1, no. 9, p. e1500396, 2015.
- [10] R. Steiger, S. Bernet, and M. Ritsch-Marte, "Mapping of phase singularities with spiral phase contrast microscopy," *Optics Express*, vol. 21, no. 14, pp. 16282-16289, 2013/07/15 2013.
- [11] B. Thidé, H. Then, J. Sjöholm, K. Palmer, J. Bergman, T. D. Carozzi, Y. N. Istomin, N. H. Ibragimov, and R. Khamitova, "Utilization of Photon Orbital Angular Momentum in the Low-Frequency Radio Domain," *Physical Review Letters*, vol. 99, no. 8, p. 087701, 08/22/2007.
- [12] M. Ibrahimi. (2017). *How do I generate OAM waves using MATLAB?* Available: https://www.quora.com/How-do-I-generate-OAM-waves-using-MATLAB
- [13] M. Abramowitz and I. A. Stegun, *Handbook of Mathematical Functions with Formulas, Graphs, and Mathematical Tables* (Applied Mathematics Series). Washington D.C.: Dover Publications, 1983.
- [14] D. Orfeo, W. Ezequille, T. Xia, and D. Huston, *Orbital angular momentum assisted ground penetrating radars* (SPIE Defense + Commercial Sensing). SPIE, 2019.
- [15] L. Allen, M. Beijersbergen, R. Spreeuw, and J. Woerdman, "Orbital angular momentum of light and transformation of Laguerre Gaussian Laser modes," *Physical review. A*, vol. 45, pp. 8185-8189, 07/01 1992.
- [16] K. Liu, Y. Cheng, Z. Yang, H. Wang, Y. Qin, and X. Li, "Orbital-Angular-Momentum-Based Electromagnetic Vortex Imaging," *IEEE Antennas and Wireless Propagation Letters*, vol. 14, pp. 711-714, 2015.
- [17] S. M. Mohammadi, L. K. S. Daldorff, J. E. S. Bergman, R. L. Karlsson, B. Thide, K. Forozesh, T. D. Carozzi, and B. Isham, "Orbital Angular Momentum in Radio—A System Study," *IEEE Transactions on Antennas and Propagation*, vol. 58, no. 2, pp. 565-572, 2010.
- [18] S. M. Mohammadi, L. K. S. Daldorff, K. Forozesh, B. Thidé, J. E. S. Bergman, B. Isham, R. Karlsson, and T. D. Carozzi, "Orbital angular momentum in radio: Measurement methods," *Radio Science*, vol. 45, no. 04, pp. 1-14, 2010.

- [19] C. Warren, A. Giannopoulos, and I. Giannakis, "gprMax: Open source software to simulate electromagnetic wave propagation for Ground Penetrating Radar," *Computer Physics Communications*, vol. 209, pp. 163-170, 2016/12/01/2016.
- [20] L. Gong, Q. Zhao, H. Zhang, X.-Y. Hu, K. Huang, J.-M. Yang, and Y.-M. Li, "Optical orbital-angular-momentum-multiplexed data transmission under high scattering," *Light: Science & Applications*, vol. 8, no. 1, p. 27, 2019/03/06 2019.
- [21] G. Berkhout, M. Lavery, M. Padgett, and M. Beijersbergen, "Measuring orbital angular momentum superpositions of light by mode transformation," *Optics letters*, vol. 36, pp. 1863-5, 05/15 2011.
- [22] A. Hassanien, M. G. Amin, E. Aboutanios, and B. Himed, "Dual-Function Radar Communication Systems: A Solution to the Spectrum Congestion Problem," *IEEE Signal Processing Magazine*, vol. 36, no. 5, pp. 115-126, 2019.